

The Warped Disc of NGC 4258

Rebecca G. Martin

University of Cambridge, Institute of Astronomy, The Observatories, Madingley Road, Cambridge CB3 0HA

ABSTRACT

We consider the properties of the warped accretion disc in NGC 4258 which is delineated by maser emission. We use our analytical models to consider whether the disc could be warped by Lense-Thirring precession. We show that such models fit the shape of the disc well and we determine the goodness of fit for various combinations of the warp radius and the disc and black hole configurations. Though the fits are compelling evidence, we note that such a model has implications for the formation and longevity of the disc which might be problematic for the current understanding of Seyfert Galaxies.

Key words: accretion, accretion discs – galaxies: active – galaxies: jets

1 INTRODUCTION

NGC 4258 is a bright barred-spiral galaxy at a distance of 7.2 Mpc (Herrnstein et al. 1999). It is in Seyfert’s first catalogue of active galaxies (Seyfert 1943). It has anomalous spiral arms of $H\alpha$ emission (Courtès & Cruvellier 1961) in the inner regions which are symmetric with respect to the nucleus. This emission is probably from shocks formed where the matter ejected from the nucleus meets the interstellar medium (van der Kruit, Oort & Mathewson 1972; Ford et al. 1986).

Masers are the microwave equivalent of lasers. Water vapour maser emission at a wavelength of 1.35 cm provides information about the accretion discs around highly compact objects in the centres of active galaxies. Masers are bright where there is no gradient in the bulk line-of-sight velocity (Grinin & Grigor’ev 1983; Watson & Wyld 2000). In a nearly edge-on Keplerian accretion disc the strongest features occur along the line to the disc centre where the disc is moving perpendicular to the line of sight, these are the systemic masers. We also see masers where the plane of the sky intersects the disc, these are the high-velocity masers.

Masers were first detected in the galaxy NGC 4258 by Claussen, Heiligman & Lo (1984) and Henkel et al. (1984). The structure and dynamics of these discs can be accurately probed with very long baseline interferometry because the emission lines are strong and intrinsically narrow. NGC 4258 has a set of masers that might trace out a warped accretion disc which is seen nearly edge on (Miyoshi et al. 1995; Herrnstein et al. 2005). Radio interferometry has shown that their rotation is Keplerian (Nakai, Inoue & Miyoshi 1993) and that the disc extends from 2.8 mas to 8.2 mas from the nucleus.

At its distance of 7.2 Mpc, in the plane of the sky we have the scaling $1 \text{ mas} = 1.077 \times 10^{17} \text{ cm} = 0.0349 \text{ pc}$. The

Keplerian rotation of the high velocity masers implies an enclosed mass of $3.78 \times 10^7 M_{\odot}$ within 2.8 mas of the nucleus (Herrnstein, Greenhill & Moran 1996). This is consistent with a central supermassive black hole.

On a scale of milliarcsseconds the central core breaks up into a jet oriented along the axis of the water maser disc (Herrnstein et al. 1997, 1998). The northern jet has a flux of 3 mJy and its mean location is about 0.4 mas north (in the plane of the sky) of the implied position of the black hole which is the centre of the rotation of the masers. However the jet position varies in time. The southern jet has not varied in flux or position and is located about 1.0 mas south of the black hole position. It has a flux of 0.5 mJy. The free-free absorption in the masing disc causes the difference in brightness between the jets (Herrnstein et al. 1997). The position angles of the jets are poorly determined. We estimate the northern jet is at a position angle of $5^{\circ} \pm 15^{\circ}$ measured from Herrnstein et al. (1998). The jets do not appear to be very well aligned with each other and the southern jet is at a position angle of about 173° . On larger scales the jet appears to be orientated north-south (Cecil et al. 2000).

The systemic masers are about 0.57 mas below the disc centre as indicated by the high velocity masers (Herrnstein et al. 2005) and at a disc radius of 3.9 mas. Hence, the masers at the inner edge of the disc suggest that it is inclined at an angle of $\zeta_{\text{in}} = \sin^{-1}(0.57/3.9) \approx 8.4^{\circ}$ to the plane of the sky. There appears to be no structure to the vertical positions of the masers in the disc and so the disc is probably thin (Miyoshi et al. 1995).

Masers operate when the temperature of the surface layers in the disc is greater than 300 K but less than 1000 K (Moran et al. 1995). The outer edge of the disc is where the molecular to atomic transition occurs, just outside the outer

maser. The reason for the apparent inner edge of the maser disc is not yet known.

The high-velocity masers are not colinear with the systemic masers and have negligible accelerations (Greenhill et al. 1995). The radial dependence of declination with respect to the systemic velocity of NGC 4258 is anti-symmetric in the red and blue-shifted masers (Miyoshi et al. 1995). It is suggested that the rotation axis of the disc varies with radius by an angle of up to 0.2 radians (Herrnstein, Greenhill & Moran 1996) and so the disc is warped. Herrnstein et al. (2005) found that the maser spots show a deviation from Keplerian rotation of about 9 km s^{-1} . They modelled this with a warped Keplerian accretion disc with a radial gradient in its inclination of 0.034 mas^{-1} .

There are several suggested explanations for the origin of the warp in the disc. Caproni et al. (2006) considered some mechanisms for the warping and precession of galactic accretion discs. Papaloizou, Terquem & Lin (1998) showed that it could be produced by a binary companion orbiting outside the maser disc. Such a companion would need a mass comparable to that of the disc but there is no observational evidence for it. A second suggestion is that radiation pressure from the central black hole produces torques on a slightly warped disc and the warp grows (Pringle 1996). However the masing disc is stable against this radiation instability if $\alpha_1 \leq 0.2$ (Caproni et al. 2007), where α_1 is the viscosity parameter (Shakura & Sunyaev 1973).

Alternatively, in the absence of other torques, Caproni et al. (2007) concluded that the warping in the disc of NGC 4258 is due to the Bardeen-Petterson effect. If we have an accretion disc around a misaligned spinning black hole, Lense-Thirring precession drives a warp in the disc. The inner parts of the disc are aligned with the black hole (Bardeen & Petterson 1975).

Caproni et al. (2007) found that the warp radius in the disc is comparable to or smaller than the radius of the inner masers. They find the timescale of alignment of the system to be a few billion years. They based their work on the results of Scheuer & Feiler (1996) who assumed that the surface density is constant. We use the more realistic power law surface density and viscosities described by Martin, Pringle & Tout (2007). We fit these analytical disc models, warped by the Lense-Thirring effect to the shape of the observed maser distribution.

2 STEADY STATE DISC MODEL

In this Section we consider some properties of accretion discs. We assume that we have a steady state disc where $\nu_1 \Sigma = \text{const}$ and that the surface density is a power law

$$\Sigma = \Sigma_0 \left(\frac{R}{R_0} \right)^{-\beta} \quad (1)$$

(Shakura & Sunyaev 1973). To be in steady state, the viscosity must obey

$$\nu_1 = \nu_{10} \left(\frac{R}{R_0} \right)^\beta, \quad (2)$$

where β , Σ_0 and ν_{10} are constants and R_0 is some fixed radius.

According to Shakura & Sunyaev (1973) the thickness of the disc in the gas pressure dominated region has

$$H \propto r^{\frac{21}{20}} (1 - r^{-\frac{1}{2}})^{\frac{1}{5}} \quad (3)$$

where $r = R/3R_g$ and $R_g = 2GM_{\text{BH}}/c^2$. This is well approximated by $H/R = \text{const}$ for $R \gg R_g$. For NGC 4258 $R_g = 1.05 \times 10^{-3} \text{ mas}$ which is much smaller than the inner edge of the disc at 2.8 mas and so we assume that $H/R = \text{const}$ in our work.

2.1 Viscosities

There are two viscosities: ν_1 corresponds to the azimuthal shear (the viscosity normally associated with accretion discs) and ν_2 corresponds to the vertical shear in the disc which smooths out the twist. The second viscosity acts when the disc is non-planar. We assume that the second viscosity obeys the same power law as ν_1 so

$$\nu_2 = \nu_{20} \left(\frac{R}{R_0} \right)^\beta \quad (4)$$

and ν_{20} is a constant.

We use the α -prescription to describe the viscosities in the disc so that

$$\nu_1 = \alpha_1 c_s H = \alpha_1 H^2 \Omega \quad (5)$$

where H is the scale height in the disc and Ω is the angular velocity and similarly

$$\nu_2 = \alpha_2 c_s H = \alpha_2 H^2 \Omega, \quad (6)$$

where

$$\alpha_1 = \alpha_{10} \left(\frac{R}{R_0} \right)^x \quad \text{and} \quad \alpha_2 = \alpha_{20} \left(\frac{R}{R_0} \right)^x, \quad (7)$$

with α_{10} , α_{20} and x constant (see below) and R_0 is some fixed radius which we define in Section 3.1. We generally take $\alpha_{10} = 0.2$ and $\alpha_{20} = 2$ (Lodato & Pringle 2007). The angular velocity in the disc is Keplerian so that

$$\Omega = \left(\frac{GM_{\text{BH}}}{R^3} \right)^{\frac{1}{2}}. \quad (8)$$

Because $c_s = H\Omega$ the azimuthal shear viscosity is

$$\begin{aligned} \nu_1 &= \alpha_1 \left(\frac{H}{R} \right)^2 R^2 \Omega \\ &= \alpha_{10} (GM_{\text{BH}} R_0)^{\frac{1}{2}} \left(\frac{H}{R} \right)^2 \left(\frac{R}{R_0} \right)^{x+\frac{1}{2}}. \end{aligned} \quad (9)$$

This can be written in the form of equation (2) with $x = \beta - \frac{1}{2}$ which is a constant and so

$$\nu_{10} = \alpha_{10} (GM_{\text{BH}} R_0)^{\frac{1}{2}} \left(\frac{H}{R_0} \right)^2. \quad (10)$$

We can find a similar equation for the vertical shear viscosity, ν_2 .

2.2 Surface Density

We let the surface density be the power law given by equation (1) but we need to find Σ_0 . We have the equation describing the hydrostatic equilibrium in the disc

$$\frac{dP}{dz} = -\rho g_z, \quad (11)$$

where P is the pressure and g_z is the z component of the gravitational force, ρ is the density and the equation of state is

$$P = \rho c_s^2, \quad (12)$$

in the case of a vertically isothermal model with c_s the, constant in z , sound speed. We find the z -component of the gravitational force to be

$$g_z = \frac{GM_{\text{BH}}z}{(R^2 + z^2)^{3/2}} \approx \frac{GM_{\text{BH}}z}{R^3} \quad (13)$$

for $z \ll R$. We can integrate equation (11) over z using equations (12) and (13) to find the pressure

$$P = P_0 \exp \left[-\frac{z^2}{2} \frac{GM_{\text{BH}}}{c_s^2 R^3} \right] \quad (14)$$

and density

$$\rho = \rho_0 \exp \left[-\frac{z^2}{2} \frac{GM_{\text{BH}}}{c_s^2 R^3} \right], \quad (15)$$

where P_0 and ρ_0 are the pressure and density at the mid-plane $z = 0$. We can now find the surface density

$$\Sigma = \int_{-\infty}^{\infty} \rho dz = \sqrt{2\pi} H \rho_0 \quad (16)$$

because

$$H = c_s \left(\frac{R^3}{GM_{\text{BH}}} \right)^{1/2}. \quad (17)$$

For a steady state accretion disc we have

$$\dot{M} = 3\pi\nu_1\Sigma, \quad (18)$$

with ν_1 the usual viscosity. We eliminate Σ from equations (16) and (18) to find

$$\rho_0 = \frac{\dot{M}}{3\pi\sqrt{2\pi}\nu_1 H} = \frac{GM_{\text{BH}}\dot{M}}{3\pi\sqrt{2\pi}\alpha_1 c_s^3 R^3} \quad (19)$$

(Neufeld & Maloney 1995) and, using equation (16), we find

$$\Sigma = \frac{\dot{M}}{3\pi\alpha_1} \left(\frac{R}{H} \right)^2 \frac{1}{(GM_{\text{BH}}R)^{1/2}}. \quad (20)$$

If $H/R = \text{const}$ then this is equivalent to

$$\Sigma = \Sigma_0 \left(\frac{R}{R_0} \right)^{-(\frac{1}{2}+x)}, \quad (21)$$

where R_0 is some fixed radius and

$$\Sigma_0 = \frac{\dot{M}}{3\pi\alpha_{10}} \left(\frac{R}{H} \right)^2 \frac{1}{(GM_{\text{BH}}R_0)^{1/2}}. \quad (22)$$

We have $\nu_1\Sigma = \text{const}$ which is necessary for a steady state disc.

2.3 Inclination of the Disc

Following Martin, Pringle & Tout (2007) we consider the disc to be made up of annuli of width dR and mass $2\pi\Sigma R dR$ at radius R from the central object of mass M_{BH} with surface density $\Sigma(R, t)$ at time t and with angular momentum $\mathbf{L} = (GM_{\text{BH}}R)^{1/2}\Sigma\mathbf{l} = L\mathbf{l}$. The unit vector describing the direction of the angular momentum of a disc annulus is given by $\mathbf{l} = (l_x, l_y, l_z)$ with $|\mathbf{l}| = 1$.

We use equation (2.8) of Pringle (1992) setting $\partial\mathbf{L}/\partial t = 0$ and adding a term to describe the Lense-Thirring precession (the last one) to give

$$0 = \frac{1}{R} \frac{\partial}{\partial R} \left[\left(\frac{3R}{L} \frac{\partial}{\partial R} (\nu_1 L) - \frac{3}{2} \nu_1 \right) \mathbf{L} + \frac{1}{2} \nu_2 R L \frac{\partial \mathbf{l}}{\partial R} \right] + \frac{\boldsymbol{\omega}_{\text{PT}} \times \mathbf{L}}{R^3}. \quad (23)$$

The Lense-Thirring precession is given by

$$\boldsymbol{\omega}_{\text{PT}} = \frac{2G\mathbf{J}}{c^2} \quad (24)$$

(Kumar & Pringle 1985), where the angular momentum of the black hole $\mathbf{J} = J\mathbf{j}$ with $\mathbf{j} = (j_x, j_y, j_z)$ and $|\mathbf{j}| = 1$ can be expressed in terms of the dimensionless spin parameter a such that

$$J = acM_{\text{BH}} \left(\frac{GM_{\text{BH}}}{c^2} \right). \quad (25)$$

We use the frame of the black hole with the black hole at the origin and with its spin along the z axis so that $\mathbf{J} = (0, 0, J)$. In this frame, Martin, Pringle & Tout (2007) find the steady state solution of equation (23) for $W = l_x + il_y$, with $i = \sqrt{-1}$, to be

$$W(R) = \frac{2W_\infty}{\Gamma\left(\frac{1}{2(1+\beta)}\right)} \frac{(-i)^{\frac{1}{4(1+\beta)}}}{(1+\beta)^{\frac{1}{2(1+\beta)}}} \left(\frac{R_0}{R} \right)^{1/4} \times K_{\frac{1}{2(1+\beta)}} \left(\frac{\sqrt{2}}{1+\beta} (1-i) \left(\frac{R}{R_0} \right)^{-\frac{1+\beta}{2}} \right), \quad (26)$$

where W_∞ is the constant value of W as $R \rightarrow \infty$. It represents the direction of the angular momentum of the outer disc. This solution has the outer disc angular momentum vector in the x - z plane. Here K_ν is the modified Bessel function of order ν and Γ is the gamma function. In deriving this solution we assume that we can neglect the non-linear term $\mathbf{l} \cdot \partial^2 \mathbf{l} / \partial R^2 = -|\partial \mathbf{l} / \partial R|^2$. We need the warping to be gradual enough for this to be true.

We let the outer disc have the fixed angular momentum direction vector $(l_{x\infty}, 0, l_{z\infty})$. As $R \rightarrow \infty$, $W \rightarrow W_\infty = l_{x\infty} = \sin \eta$ where η is the inclination of the outer disc to the black hole. The inclination of the disc to the black hole at radius R (the z -axis) is

$$\theta(R) = \cos^{-1}(l_z) = \cos^{-1}(\sqrt{1 - |W|^2}). \quad (27)$$

We let the angle ϕ be the usual azimuthal angle in spherical polar coordinates with $0 \leq \phi < 2\pi$. It is the angle in the x - y plane from the projected direction of the outer disc angular momentum which in our model, given by equation (26), is along the x -axis.

2.4 Disc Section

The high velocity masers trace the disc in NGC 4258 in the plane of the sky so we need to find the cross section of our disc model in this plane. Our solution is in coordinates (x, y, z) in the frame of the black hole and the outer disc lies in the x - z plane. We initially take this to be aligned with the coordinates $(x_{\text{bh}}, y_{\text{bh}}, z_{\text{bh}})$ which are the coordinates that we take the disc section in the $x_{\text{bh}}-z_{\text{bh}}$ plane.

We rotate the coordinates (x, y, z) about the z_{bh} axis by

an angle $-\phi_c$. The shape of the disc in the $x_{\text{bh}}-z_{\text{bh}}$ plane is given by

$$z_{\text{bh}}(R) = -\frac{R}{R_0} \tan \theta \cos(\phi_c - \phi_{\text{max}}), \quad (28)$$

where $\phi_{\text{max}} = \arg(W)$ and we have the negative sign so that our model has the same orientation as the maser data and

$$x_{\text{bh}}(R) = \frac{R}{R_0} (\sin^2(\phi_c - \phi_{\text{max}}) + \cos^2 \theta \cos^2(\phi_c - \phi_{\text{max}}))^{\frac{1}{2}} \quad (29)$$

in the positive x_{bh} direction. We are assuming that the disc is symmetric so the side of the disc with negative x_{bh} can be found by rotating this shape by 180° about the y_{bh} axis.

If $\phi_c = 0$ we see the largest warp possible for a given disc because we are taking a disc section in the plane which contains both the black hole and the outer disc angular momentum. Conversely, if $\phi_c = \pi/2$ then we see the least warping in our disc section.

We next consider the disc section when the black hole is not in the plane of the sky but inclined at angle i_{inc} to it. We rotate the (x, y, z) coordinates about the x_{bh} axis through an angle $-i_{\text{inc}}$. For small i_{inc} the shape of our disc becomes

$$z_{\text{bh}}(R) = -\frac{R}{R_0} \tan \theta \cos(\phi_c - \phi_{\text{max}}) \cos i_{\text{inc}} \quad (30)$$

and x_{bh} remains the same. If the plane of the sky contains the black hole spin then $i_{\text{inc}} = 0$. We can use this small angle approximation because if the angle i_{inc} were big then we wouldn't see the masers because they are only seen when there is no gradient in the bulk line of sight velocity. This only happens when the disc is close to edge on.

We sketch the plane of the sky coordinates $(x_{\text{bh}}, z_{\text{bh}})$ and the coordinate system for the disc (x, y, z) in Figure 1. We show the plane of the sky, P , in which we find the disc section. It contains the dashed lines. The normal, \mathbf{n} , to the plane P is the line of sight. The disc section is in coordinates x_{bh} and z_{bh} .

In the case where $i_{\text{inc}} = 0$ and $\phi_c = 0$, we find the inclination of the disc at radius R to the plane of the sky to be

$$\zeta = \pi/2 - \cos^{-1}(l_y). \quad (31)$$

The observations of the systemic masers predict that, at $R = 3.9 \text{ mas}$, the disc has inclination $\zeta_{\text{in}} = 8.4^\circ$. For our models with $i_{\text{inc}} = 0$ and $\phi_c = 0$ we find the inclination of our disc at $R = 3.9 \text{ mas}$ and compare this to the observed value.

3 PROPERTIES OF NCG 4258

The inner radius of the masing disc corresponds to $R_{\text{in}} = 2.8 \text{ mas}$ and the outer edge to $R_{\text{out}} = 8.2 \text{ mas}$. Argon et al. (2007) examine the systemic masers in the direction perpendicular to the axis of the disc. They observe that the vertical thickness of the disc has a limit $H < 0.005 \text{ mas}$. Because the systemic masers are at $R = 3.9 \text{ mas}$ we see there is an observed upper limit on H/R such that

$$\frac{H}{R} < 0.0013. \quad (32)$$

We use a canonical value of $H/R = 0.001$ in the following calculations.

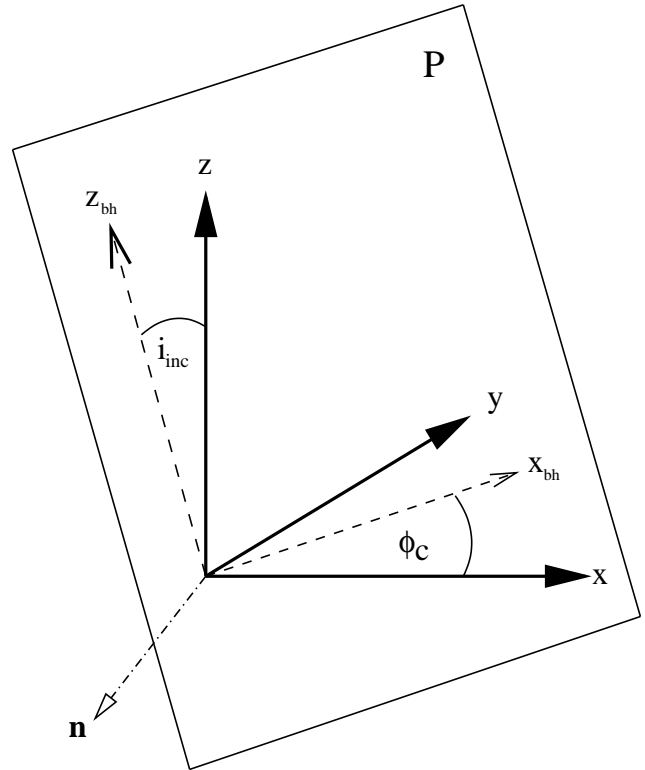


Figure 1. A diagram showing the plane of the sky, P , with normal \mathbf{n} which corresponds to the line of sight. We find the disc section in the plane P . The Cartesian coordinates used for the general solution to the warped disc equation given by equation (26) are (x, y, z) . The black hole spin is up the z axis and the outer disc angular momentum is in the $x-z$ plane. The coordinates in the plane of the sky are x_{bh} and z_{bh} , and y_{bh} is in the direction of $-\mathbf{n}$. To find the orientation of the black hole and the disc we start with (x, y, z) aligned with $(x_{\text{bh}}, y_{\text{bh}}, z_{\text{bh}})$. We then rotate x and y about the z_{bh} axis by an angle $-\phi_c$. Then we rotate about the x_{bh} axis by an angle $-i_{\text{inc}}$. The dashed lines are in the plane, P .

3.1 Warp Radius

The warp radius is where the Bardeen-Petterson effect is balanced by the viscous evolution of the disc and is given by

$$R_{\text{warp}} = 2 \frac{\omega_p}{\nu_2(R_{\text{warp}})} \quad (33)$$

(Scheuer & Feiler 1996; Martin, Pringle & Tout 2007), where $\omega_p = |\omega_p|$. Using equation (24) and the form of equation (9) for the second viscosity we find

$$R_{\text{warp}} = \frac{4aG^2M_{\text{BH}}^2}{c^3\alpha_{20}R_{\text{warp}}^2} \left(\frac{R}{H}\right)^2 \left(\frac{R_{\text{warp}}^3}{GM_{\text{BH}}}\right)^{\frac{1}{2}} \quad (34)$$

and, rearranging,

$$R_{\text{warp}} = \left[\frac{4a(GM_{\text{BH}})^{\frac{3}{2}}}{c^3\alpha_{20}} \left(\frac{R}{H}\right)^2 \right]^{\frac{2}{3}}. \quad (35)$$

More specifically, for NGC 4258 we find

$$R_{\text{warp}} = 0.83 a^{\frac{2}{3}} \left(\frac{\alpha_{20}}{2}\right)^{-\frac{2}{3}} \left(\frac{H/R}{0.001}\right)^{-\frac{4}{3}} \text{ mas}. \quad (36)$$

This warp radius is closer to the black hole than the inner masers and we consider this in more detail in Section 3.4.

3.2 Accretion rate

The motion of the infalling gas in NGC 4258 cannot be measured directly so we have to estimate the mass accretion rate, \dot{M} , indirectly. We use the bolometric luminosity of the system and assume that

$$L_{\text{bol}} = \epsilon \dot{M} c^2, \quad (37)$$

where ϵ is the accretion efficiency of a Kerr black hole, $\epsilon \approx 0.1$. The bolometric luminosity of NGC 4258 is about $4 \times 10^{42} \text{ erg s}^{-1}$. This corresponds to a mass accretion rate of

$$\dot{M} = 7 \times 10^{-5} M_{\odot} \text{ yr}^{-1} \quad (38)$$

if the disc is in a steady state.

3.3 Surface Density and Mass of the Disc

We explore the consequences of the assumption that the disc is in steady state. When we vary β we want properties of the disc at $R = R_{\text{warp}}$ to be fixed and so we choose $R_0 = R_{\text{warp}}$. We find the surface density using equation (21) to be

$$\Sigma = \Sigma_0 \left(\frac{R}{R_{\text{warp}}} \right)^{-(x+\frac{1}{2})}, \quad (39)$$

where

$$\begin{aligned} \Sigma_0 &= \frac{\dot{M}}{3\pi\alpha_1} \left(\frac{R}{H} \right)^2 \frac{1}{(GM_{\text{BH}}R_{\text{warp}})^{\frac{1}{2}}} \\ &= 1.11 \times 10^2 \left(\frac{\alpha_{10}}{0.2} \right)^{-1} \left(\frac{\alpha_{20}}{2} \right)^{\frac{1}{3}} a^{-\frac{1}{3}} \left(\frac{H/R}{0.001} \right)^{-\frac{4}{3}} \\ &\quad \times \left(\frac{\dot{M}}{7 \times 10^{-5} M_{\odot} \text{ yr}^{-1}} \right) \text{ g cm}^{-2}. \end{aligned} \quad (40)$$

Caproni et al. (2007) used the same model for the disc with $\alpha_1 = \text{const}$ but varied H/R with a power law in R .

Using the surface density of the disc we can find the total mass of the observable disc to be

$$M_{\text{d}} = 2\pi \int_{R_{\text{in}}}^{R_{\text{out}}} \Sigma R dR = \frac{2\pi\Sigma_0}{2-\beta} R_{\text{warp}}^{\beta} (R_{\text{out}}^{2-\beta} - R_{\text{in}}^{2-\beta}) \quad (41)$$

if $\beta \neq 2$, or, if $\beta = 2$ then

$$M_{\text{d}} = 2\pi\Sigma_0 R_{\text{warp}}^2 \log \left(\frac{R_{\text{out}}}{R_{\text{in}}} \right). \quad (42)$$

For NGC 4258, with $\beta = 2$, we find

$$\begin{aligned} M_{\text{d}} &= 2.97 \times 10^3 a \left(\frac{\alpha_{10}}{0.2} \right)^{-1} \left(\frac{\alpha_{20}}{2} \right)^{-1} \left(\frac{H/R}{0.001} \right)^{-4} \\ &\quad \times \left(\frac{\dot{M}}{7 \times 10^{-5} M_{\odot} \text{ yr}^{-1}} \right) M_{\odot}. \end{aligned} \quad (43)$$

This is much smaller than the mass of the black hole but in the next section we consider if this is, or could be, large enough for our disc to be self-gravitating.

3.4 Self Gravity of the Disc

Having calculated the mass of the observed maser disc we check if the disc is stable against the effects of self gravity. If it were unstable against self gravity then it would collapse

into bound fragments locally. If the mass of the disc satisfies the inequality

$$M_{\text{d}} < M_{\text{BH}} \left(\frac{H}{R} \right) \quad (44)$$

then the disc is stable (Toomre 1964; Binney & Tremaine 1987). For $H/R = 0.001$ this corresponds to a critical disc mass of $3.78 \times 10^4 M_{\odot}$. For $\beta = 2$, using equation (43), we see that we need $H/R > 0.0006$ for a disc which is stable against self gravity. Now we have constrained H/R to the approximate limits of

$$0.0006 < H/R < 0.0013 \quad (45)$$

if our model is correct. Using equation (36) we find that for $\beta = 2$ our warp radius is limited to

$$0.58 < \frac{R_{\text{warp}}}{1 \text{ mas}} < 1.65. \quad (46)$$

This is a relatively small range. We note that this range for R_{warp} is completely inside the inner observed maser points. Caproni et al. (2007) found that the warp radius was approximately equal to or smaller than the inner maser but we find that it is at most around half way between the black hole and the inner maser.

We note that this mass just takes into account the mass of the disc of the observed masers. For our steady state solution, the surface density increases as we move towards the black hole and so, if we calculate the mass of the disc including inner regions, then our disc soon becomes self-gravitating. If the inner parts of the disc were not in steady state or if H/R were much larger there then we could overcome this problem.

3.5 Gravitational Torques

In our model, different radii of the disc communicate through the two viscosities. Discs of non-negligible mass could also communicate through gravitational torques. We consider here how these torques would affect equation (23). Nayakshin (2005) considered the gravitational torque between two rings at radii R and R_1 of masses M and M_1 respectively which are inclined at an angle γ to each other. The torque exerted by the second ring on the first is

$$T_{\text{grav}} = \frac{GM_1M}{4\pi^2} \int_0^{2\pi} \int_0^{2\pi} \frac{|\mathbf{r}_1 \times \mathbf{r}|}{|\mathbf{r} - \mathbf{r}_1|^3} d\phi d\phi_1, \quad (47)$$

where \mathbf{r} and \mathbf{r}_1 are the position vectors around the rings and the integration goes over ϕ and ϕ_1 which are azimuthal angles in the frame of the respective rings. He found the maximum precession frequency to be when $R/R_1 = \sqrt{3/7}$ and the maximum torque to be

$$\begin{aligned} T_{\text{grav}} &= 0.085 M\Omega^2 R^2 \sin \gamma \cos \gamma \frac{M_1}{M_{\text{BH}}} \\ &= 0.085 M\Omega^2 R^2 \sin \gamma \cos \gamma \frac{2\pi R_1 \Sigma_1 \delta R_1}{M_{\text{BH}}}, \end{aligned} \quad (48)$$

where $M_1 = 2\pi\Sigma_1 R_1 \delta R_1$ is the mass of an inclined annulus on which we consider the torque and $\Sigma_1 = \Sigma(R_1)$. In this formula M is the mass of the annulus at R which provides the greatest torque. We replace M by the mass of the disc, M_{d} to obtain an upper limit on the total torque on the annulus at R_1 .

The magnitude of the viscous torque is (equation (23))

$$\begin{aligned} T'_{\text{visc}} &= \frac{1}{R_1^2} \frac{1}{2} \nu_2(R_1) R_1 L_1 \left| \frac{\partial l}{\partial R} \right|_1 \\ &= \frac{1}{2R_1^2} \nu_2(R_1) L_1 \sin \gamma \end{aligned} \quad (49)$$

because

$$R_1 \left| \frac{\partial l}{\partial R} \right|_1 = \sin \gamma. \quad (50)$$

We multiply by the area of the ring to find the viscous torque acting on a ring of width δR_1 at radius R_1 to be

$$T_{\text{visc}} = 2\pi R_1 \delta R_1 \frac{1}{2R_1^2} \nu_2(R_1) L_1 \sin \gamma. \quad (51)$$

We now compare the magnitude of the maximum gravitational torque to the viscous torque

$$\xi_{\text{grav}} = \frac{T_{\text{grav}}}{T_{\text{visc}}} = \frac{0.085 M_d \Omega^2 R^2 R_1 \sin \gamma \cos \gamma \frac{2\pi R_1 \Sigma_1}{M_{\text{BH}}}}{\pi \nu_2(R_1) L_1 \sin \gamma} \quad (52)$$

and substituting we find

$$\begin{aligned} \xi_{\text{grav}} &= \frac{T_{\text{grav}}}{T_{\text{visc}}} = \frac{0.085 M_d \Omega^2 R^2 R_1 \sin \gamma \cos \gamma \frac{2\pi R_1 \Sigma_1}{M_{\text{BH}}}}{\pi \nu_2(R_1) (GM_{\text{BH}} R_1)^{\frac{1}{2}} \Sigma_1 \sin \gamma} \\ &= \frac{0.17 M_d G R_1^2 \cos \gamma}{\nu_2(R_1) R (GM_{\text{BH}} R_1)^{\frac{1}{2}}} \\ &= \frac{0.17 M_d R_1^2 \cos \gamma}{\nu_{20} R (G^{-1} M_{\text{BH}} R_1)^{\frac{1}{2}}} \left(\frac{R_1}{R_{\text{warp}}} \right)^{-\beta}. \end{aligned} \quad (53)$$

With $\beta = 2$ and $\cos \gamma \approx 1$ at $R = R_{\text{in}}$ and $R_1 = \sqrt{7/3} R_{\text{in}}$ we find that $\xi_{\text{grav}} = 3 \times 10^{-4} (M_d/M_{\odot})$ and at $R_1 = R_{\text{out}}$ and $R = \sqrt{3/7} R_1$ then $\xi_{\text{grav}} = 10^{-4} (M_d/M_{\odot})$. Using the disc mass derived in Section 3.3 of $M_d = 3 \times 10^3 M_{\odot}$ we find at $R = R_{\text{in}}$, $\xi_{\text{grav}} = 0.9$ and at $R_1 = R_{\text{out}}$, $\xi_{\text{grav}} = 0.3$. This disc mass is the critical one at which the gravity torques become as important as the viscous torques. For smaller disc masses self gravity torques would be unimportant. In any case the gravitational torque is not as large as the viscous torque even at its maximum so we are justified in neglecting it. However, it ought to be included in any numerical models especially for larger disc masses.

4 COMPARING THE MODEL TO OBSERVATIONS

In this section we compare the maser data to our analytical disc models and find parameters which give the best fits.

4.1 Maser Data

We use the maser distribution data tabulated in the online version of Argon et al. (2007). This lists positions of each maser in the plane of the sky, z_m and x_m . For the first set of data, BM056C, we correct the north-south position of the masers (Alice Argon, private communication). They correlated the first three epochs at a less accurate position than later epochs and the data in the online table for BM056C reflect this. From the relativistic velocity, v_{rel} , in column 3

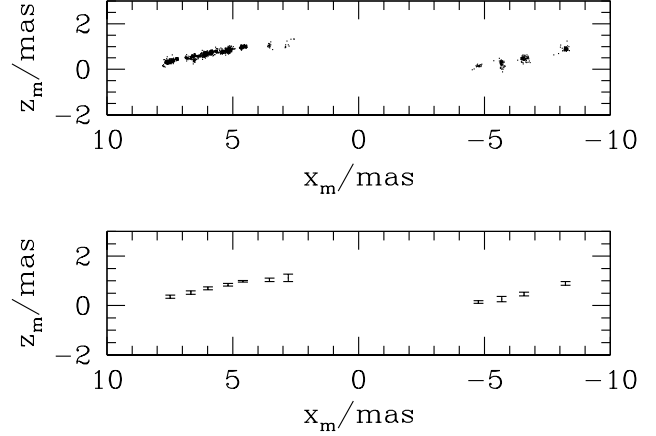


Figure 2. The maser distribution in space. The top plot shows all the data points and the bottom plot shows the binned data with error bars.

of Table 5 in the online table of Argon et al. (2007), we find the frequency

$$f_{\text{freq}} = 22.23508 \left(\frac{1 - v_{\text{rel}}/c}{1 + v_{\text{rel}}/c} \right)^{1/2} \text{ GHz}, \quad (54)$$

where $c = 2.998 \times 10^{10} \text{ cm s}^{-1}$. Then we apply the correction

$$z_m \rightarrow z_m - 66.0 \left(\frac{f_{\text{freq}}}{22.19856} - 1 \right) \text{ mas} \quad (55)$$

and x_m remains the same.

In order to get an estimate of the measurement error we bin the maser data points. We put the data into 11 bins and find the average \bar{x}_i and \bar{z}_i in each where $i = 1, 2, \dots, 11$. We then find the standard deviations of each average point, σ_{ix} and σ_{iz} . We list these in Table 1. In Figure 2 we plot all of the maser data in the top plot and below we plot the binned data points with error bars.

The symmetry of the velocity distribution of the masers tells us that the black hole is on the line $x_m = 0$ and we find the position of the black hole, z_{add} , from the symmetry of the shape of the maser distribution. We use the inner three points on the right in the binned data and find an interpolated corresponding z_m value on the left hand side at the positive x_m . We can then find the midpoint of these two z_m values from the left and right hand sides. We average over the three points calculated and find that $z_{\text{add}} = 0.52$ in the frame of the masers.

4.2 Disc Section Transformation

We have the shape of the disc section as given in the coordinates z_{bh} and x_{bh} . However, we can vary the size, the rotation angle and position within the plane to get a good fit. We first let $R_0 = R_{\text{warp}} = 1 \text{ mas}$ in equation (26) and find the disc section we want.

We rotate this disc section by an angle q about the line of sight. The black hole spin was originally in the north-south direction but with this transformation it is at a position angle of $-q$. If we assume that the observed jets are parallel to the spin of the black hole, then the black hole spin should be at the same position angle as the jets.

i	\bar{x}_i/mas	\bar{z}_i/mas	Number of Masers	σ_{ix}	σ_{iz}
1	-8.222	0.896	92	8.018×10^{-2}	7.116×10^{-2}
2	-6.574	0.465	90	9.047×10^{-2}	7.836×10^{-2}
3	-5.684	0.261	71	5.939×10^{-2}	1.094×10^{-1}
4	-4.760	0.143	24	8.717×10^{-2}	5.445×10^{-2}
5	2.796	1.120	11	1.271×10^{-1}	1.466×10^{-1}
6	3.539	1.041	19	4.210×10^{-2}	7.498×10^{-2}
7	4.598	0.985	383	7.121×10^{-2}	3.427×10^{-2}
8	5.188	0.843	1042	7.872×10^{-2}	5.321×10^{-2}
9	5.984	0.694	1499	1.510×10^{-1}	5.959×10^{-2}
10	6.666	0.528	358	1.259×10^{-1}	6.753×10^{-2}
11	7.483	0.355	666	1.484×10^{-1}	6.676×10^{-2}

Table 1. The binned maser points with the number of points in each bin and the standard deviations.

We can choose the factor $f = R_{\text{warp}}/\text{mas}$ which determines where R_{warp} is relative to the maser distribution. Our model becomes

$$z_t = \pm(z_{\text{bh}} \cos q + x_{\text{bh}} \sin q)f + z_{\text{add}} \quad (56)$$

and

$$x_t = \pm(x_{\text{bh}} \cos q - z_{\text{bh}} \sin q)f, \quad (57)$$

where the sign depends on which side of the disc we are modelling.

We now have a model which can be rotated, stretched and moved to fit the masers. We choose the parameters η , f and β for the disc we wish to fit. Then we choose a disc section by choosing ϕ_c and i_{inc} . We then rotate the disc section to the best fit by varying q .

4.3 Comparison of our Model to the Maser Data

We can compare our analytical model to the binned points by finding

$$\frac{\chi_\nu^2}{\nu} = \frac{1}{\nu} \sum_{i=1}^N \frac{(z_i - z_t)^2}{\sigma_i^2}, \quad (58)$$

where $\nu = N - m$, $N = 11$ is the number of bins and m is the number of parameters to be determined from the data. We can change the inclination of the black hole relative to the outer disc, η , and also the power β . We can rotate the disc about the axis of the black hole by changing angle ϕ_c . We can also vary the inclination, i_{inc} , of the black hole to the line of sight. We can vary the warp radius through f .

For a given set of parameters for η , β , f , i_{inc} , ϕ_c , we minimise $\chi_{10}^2/10$ by varying q . We vary one parameter at a time and so $m = 1$ and $\nu = 10$. The critical probability values, p , for deviations of 1, 2 and 3σ for $\chi_{10}^2/10$ are given in Table 2. The probability of exceeding the critical value of $\chi_{10}^2/10$ is $1 - p$.

In Figure 3 we plot contours of $\chi_{10}^2/10$ in f and η space for different values of β , ϕ_c and i . Each point in the plot is the best fitting point when we vary q . The plots would be symmetric over the line $\eta = 90^\circ$ if we were to extend them to higher η because the disc shape is the same for η and $\pi - \eta$ but if $\eta > \pi/2$ the disc is counter aligned. We see that we can fit the disc shape for a variety of parameters.

Generally, we see that we need $\eta > 30^\circ$ or so for a reasonable fit and the warp radius must be on the scale of

σ	p	$\chi_{10}^2/10$
1	0.683	1.154
2	0.955	1.865
3	0.997	2.661

Table 2. The probability of exceeding the critical value of $\chi_{10}^2/10$ is $1 - p$. We tabulate critical values of $\chi_{10}^2/10$ for deviations of 1, 2 and 3σ .

the masers. Comparing the top plots which have different β only, we see that for the lower value of $\beta = 1$ we can fit higher R_{warp} better but we cannot fit such small η as for $\beta = 2$.

The bottom left plot is the same as the top right plot except the black hole is inclined at an angle of $i_{\text{inc}} = 10^\circ$ to the plane of the sky. Comparing this to the top right plot which has $i_{\text{inc}} = 0$ we see that the the range of parameters we can fit is not changed much for small inclinations of the black hole from the plane of the sky. Note that the method we have used to generate these fits does not take into account whether masers would actually be seen for the inclinations chosen. We need the inclination of the black hole from the plane of the sky to be small in order to see masers at all.

In all the plots considered so far, we have chosen the disc section of a given disc with the most warping, the one where the plane of the sky contains the angular momentum of the black hole and outer disc vectors. In the bottom right plot we choose a different disc section with $\phi_c = 45^\circ$. Here, we cannot fit such small R_{warp} or η .

In Section 3.1 we found an upper limit on the warp radius for the disc to be stable against self gravity that R_{warp} must be less than 1.65 mas. This rules out the case with $\phi_c = 45^\circ$ completely. We find that we can only fit discs which have $|\phi_c| < 25^\circ$. In order for our models to explain the warping in NGC 4258, the black hole and outer disc angular momentum vectors must be close to lying in the the plane of the sky. By the bottom left plot, the limit also implies that we need $\eta > 60^\circ$.

4.4 Best Fitting Models

We consider the best fitting combination of parameters for the case $\beta = 2$, $i = 0$ and $\phi_c = 0$. The parameters giving the smallest $\chi_{10}^2/10$ of 0.173 are $\eta = 45.8^\circ$ and $R_{\text{warp}} = 5.8$ mas

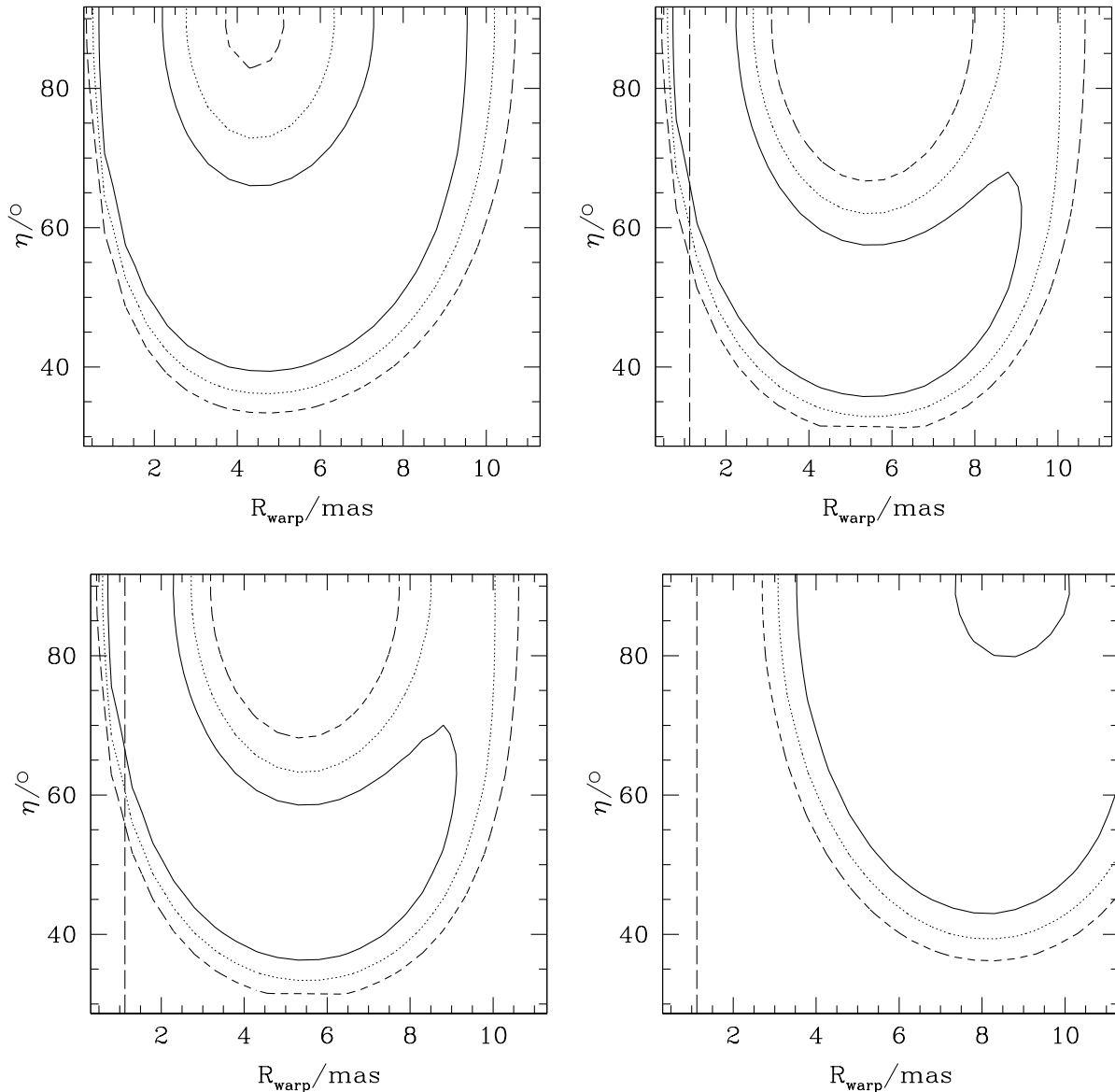


Figure 3. Contour plots of the values of $\chi_{10}^2/10$ for combinations of $R_{\text{warp}}/\text{mas}$ and η , the angle between the black hole and outer disc angular momenta. The solid lines are $\chi_{10}^2/10 = 1.154$, the dotted lines are $\chi_{10}^2/10 = 1.865$ and the dashed lines are $\chi_{10}^2/10 = 2.661$ which correspond to 1, 2 and 3 σ deviations. The top left plot has $\beta = 1$, $\phi_c = 0$ and $i_{\text{inc}} = 0$. The top right plot has $\beta = 2$, $\phi_c = 0$ and $i_{\text{inc}} = 0$. The bottom left plot has $\beta = 2$, $\phi_c = 0$ and $i_{\text{inc}} = 10^\circ$. The bottom right plot has $\beta = 2$, $\phi_c = 45^\circ$ and $i_{\text{inc}} = 0$. The vertical long dashed lines shown for the cases with $\beta = 2$ are the upper limit on R_{warp} derived from the condition that the disc must be stable against self gravity.

and this has $q = 10.6^\circ$. The position angle of the black hole is $-q$ and so if we assume that the jets are parallel to the spin of the black hole then the position angle of the jets here is -10.6° . This is on the edge of our error for the observed position angle of the jets. The inclination of the disc at $R = 3.9 \text{ mas}$ to the plane of the sky is $\zeta_{\text{in}} = 7.4^\circ$. In the top of Figure 4 we plot this fit with the maser data points. For this warp radius we would need $H/R = 0.0002$ and so the disc would be unstable against self gravity.

The best fitting model which is stable against self gravity has $R_{\text{warp}} = 1.3 \text{ mas}$, $\eta = 85.9^\circ$, $\chi_{10}^2/10 = 0.20331$ and $q = 39.6^\circ$ and we plot this in the bottom plot in Figure 4. If

we take into account our constraint on R_{warp} then we need a larger angle q which means that the black hole has position angle which is more negative and not within the error on the observed position angle of the jets. However, the inclination of the disc at $R = 7 \text{ mas}$ to the plane of the sky is $\zeta_{\text{in}} = 8.6^\circ$ which is closer to the observed value of 8.4° .

The angles of the jets are very poorly determined and vary in time indicating that the angle is affected by the surrounding medium. None of the models that fit the data well have negative q . Once we constrain the warp radius we find we need an even larger q to fit the data. However, the

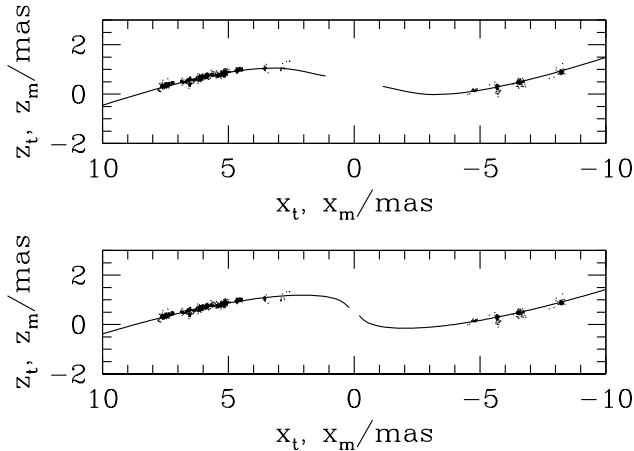


Figure 4. The maser points with the best fitting models with $\beta = 2$, $i_{\text{inc}} = 0$ and $\phi_c = 0$. The top plot has $\chi_{10}^2/10 = 0.173$, $\eta = 45.8^\circ$, $R_{\text{warp}} = 5.8 \text{ mas}$ and $q = 10.6^\circ$. The bottom plot is the best fitting model which is stable against self gravity and has $\chi_{10}^2/10 = 0.203$, $\eta = 90^\circ$, $R_{\text{warp}} = 1.3 \text{ mas}$ and $q = 39.8^\circ$.

jet is not very clearly observed (Herrnstein et al. 1997) and so we cannot rule out our models because of this.

5 PHYSICAL IMPLICATIONS FOR THE DISC

We now consider the physical implications of our fit to the disc structure in NGC 4258. First we calculate the viscous timescale in the disc. For $R_{\text{warp}} = 0.83 \text{ mas}$ with $H/R = 0.001$ we find the viscosity to be

$$\nu_1 = 4.3 \times 10^{18} \left(\frac{R}{R_{\text{warp}}} \right)^\beta \text{ cm}^2 \text{ s}^{-1}. \quad (59)$$

The viscous timescale in the disc for $\beta = 2$ is independent of R and is given by

$$t_{\nu_1} = \frac{R^2}{\nu_1} = \frac{R_{\text{warp}}^2}{\nu_{10}} = 6.3 \times 10^7 \text{ yr}. \quad (60)$$

and represents the timescale of the movement of mass through the disc. The second viscosity timescale is

$$t_{\nu_2} = \frac{\alpha_{10}}{\alpha_{20}} t_{\nu_1} = 6.3 \times 10^6 \text{ yr} \quad (61)$$

and this is the timescale associated with the generation of the warp in the disc.

The precession timescale due to the Lense-Thirring effect is given by

$$t_{\text{LT}} = \frac{c^2 R^3}{2GJ} = \frac{c^3 R^3}{2aG^2 M_{\text{BH}}^2}. \quad (62)$$

At R_{warp} we have $t_{\text{LT}} = t_{\nu_2}$ because of the definition of R_{warp} . At R_{in} , $t_{\text{LT}} = 4.6 \times 10^8 \text{ yr}$ which is longer than t_{ν_1} . Hence, for the disc to be in a steady state we require it to last for much longer than the viscous timescale. This means that the disc must be effectively of infinite mass because it is continually supplied with matter.

Seyfert outbursts are stochastic randomly-orientated, short-lived accretion events. If this system is a Seyfert system then the maser disc is just the outer regions of a disc generated by an accretion event. Seyfert episodes thought

to be shorter than 10^6 yr (Sanders 1984) and nuclei evolve through at least 100 of these. The disc becomes stable and thin in a few orbital periods, a time of around 10^3 yr at the outer edge of the disc. The warp then just represents the distribution of angular momentum in the accreted matter. The time to change the warp, around 10^8 yr , is much longer than the length of the Seyfert outburst and the typical time to the next outburst. It is hard to reconcile our model without upsetting this understanding of Seyfert outbursts.

However NGC4258 is a rather inactive AGN. The assumed luminosity is well below the Eddington luminosity. We suggest that it could be in a more quiescent phase with steady accretion.

6 CONCLUSIONS

We can fit the shape of the warped disc in NGC 4258 with steady state accretion disc which has a misaligned spinning black hole that causes the disc to warp by Lense-Thirring precession. We need the angle between the black hole and the outer disc to be greater than 60° in order to get a good fit. We need the warp radius to be $1 < R_{\text{warp}}/\text{mas} < 10$. We need the angular momentum of the outer disc to be at an angles of less than 25° to the plane of the sky. The black hole spin must be close to the plane of the sky to see masers.

The best fitting model has the warp radius at 5.8 mas and a black hole position angle of -10° but this disc would be unstable to self gravity. The best fitting model which would not be self gravitating has $R_{\text{warp}} = 1.3 \text{ mas}$ but the position angle of the black hole is -40° . The observed direction of the jet is $5^\circ \pm 15^\circ$ and so cannot be easily accounted for using this model.

We need the disc to be very long lived in order for it to become warped in its lifetime. If the disc was in steady state all the way in, it would be unstable against self-gravity. The requirements of the model are hard to fit with our understanding of Seyfert outbursts which are thought to last only 10^6 yr . However, it remains that we can fit the observed maser distribution with an accretion disc warped by Lense-Thirring precession remarkably well.

ACKNOWLEDGEMENTS

I thank Jim Pringle for many useful discussions and reading the manuscript and Christopher Tout for help with statistics and other useful discussions. I thank Alice Argon and Jim Moran for advice about the maser observations and Anderson Caproni and Lincoln Greenhill for useful comments.

REFERENCES

- Argon A. L., Greenhill L. J., Reid M. J., Moran J. M., Humphreys E. M. L., ApJ, 659, 1040
- Bardeen J. M., Petterson J. A., 1975, ApJ, 195, L65
- Binney J., Tremaine S., 1987, Galactic Dynamics, Princeton, Princeton University Press
- Caproni A., Abraham Z., Livio M., Mosquera Cuesta H. J., 2007, MNRAS, 379, 135
- Caproni A., Livio M., Abraham Z., Mosquera Cuesta H. J., 2006, ApJ, 653, 112

- Cecil et al., 2000, ApJ, 536, 675
Claussen M. J., Heiligman G. M., Lo K. Y., 1984, Nature, 310, 298
Courtès G., Cruvellier P., 1961, Compt. Rend. Acad. Sci. Paris, 253, 218
Ford H. C., Dahari O., Jacoby G. H., Crane P. C., Ciardullo R., 1986, ApJ, 311, L7
Greenhill L. J., Jiang D. R., Moran J. M., Reid M. J., Lo K. Y., Claussen M. J., 1995, ApJ, 440, 619
Grinin V. P., Grigor'ev S. A., 1983, SvA, 27, 298
Henkel C., Güsten R., Wilson T. L., Biermann P., Downes D., Thum C., 1984, A&A, 141, L1
Herrnstein J. R., Greenhill L. J., Moran J. M., 1996, ApJ, 468, L17
Herrnstein J. R., Moran J. M., Greenhill L. J., Diamond P. J., Miyoshi M., Nakai N., Inoue M., 1997, ApJ, 475, L17
Herrnstein J. R., Greenhill L. J., Moran J. M., Diamond P. J., Inoue M., Nakai N., Miyoshi M., 1998, ApJ, 497, L69
Herrnstein J. R., et al., 1999, Nat, 400, 539
Herrnstein J. R., Moran J. M., Greenhill L. J., Trotter A. S., 2005, ApJ, 629, 719
Kumar S., Pringle J. E., 1985, MNRAS, 213, 435
Lodato G., Pringle J. E., 2007, MNRAS
Martin R. G., Pringle J. E., Tout C. A., 2007, 381, 1617
Miyoshi M., Moran J. M., Herrnstein J. R., Greenhill L. J., Nakai N., Diamond P. J., Inoue M., 1995, Nature, 373, 127
Moran J., Greenhill L., Herrnstein J., Diamond P., Miyoshi M., Nakai N., Inoue M., 1995, Proc. Natl. Acad. Sci., 92, 11427
Nakai N., Inoue M., Miyoshi M., 1993, Nature, 361, 45
Nayakshin S., 2005, MNRAS, 359, 545
Neufeld D. A., Maloney P. R., 1995, ApJ, 447, L17
Papaloizou J. C. B., Terquem C., Lin D. N. C., 1998, ApJ, 497, 212
Pringle J. E., 1992, MNRAS, 258, 811
Pringle J. E., 1996, MNRAS, 281, 857
Sanders R. H., 1984, A&A, 140, 52
Scheuer P. A. G., Feiler R., 1996, MNRAS, 282, 291
Seyfert C., 1943, ApJ, 97, 28
Shakura N. I., Sunyaev R. A., 1973, A&A, 24, 337
Toomre A., 1964, ApJ, 139, 1217
van der Kruit P. C., Oort J. H., Mathewson D. S., 1972, A&A, 21, 169
Watson W. D., Wyld H. W., 2000, ApJ, 530, 207